Available online at www.sciencedirect.com
SCIENCE DIRECT®
Pergamon
Cement and Concrete Research 34 (2004) 341–348
CEMENT AND CONCRETE RESEARCH

# Dissolution-precipitation behaviour of ettringite, monosulfate, and calcium silicate hydrate

Isabel Baur*, Peter Keller[1], Denis Mavrocordatos, Bernhard Wehrli, C. Annette Johnson

*Swiss Federal Institute for Environmental Science and Technology (EAWAG), Box 611, CH-8600 Dubendorf, Switzerland*

Received 13 June 2002; accepted 14 August 2003

**Abstract**

The stability of the cement minerals ettringite, monosulfate, and calcium silicate hydrate (C-S-H) was investigated to better understand the uptake of contaminants in waste–cement mixes. Suspensions were spiked with radioisotopes of components ($^{45}Ca$ and $^{35}SO_4$ for ettringite and monosulfate and $^{45}Ca$ and $^{32}Si$ for C-S-H) to observe their uptake behaviour within 0–70 days. A physical model was applied to determine dissolution-precipitation rates. An initial fast uptake was observed to occur in most systems, so the data obtained between 7 and 70 days were chosen for analysis. Dissolution-precipitation rates were in the range of $10^{-11.5}$ to $10^{-12.2}$ mol $m^{-2}$ $s^{-1}$ for all minerals. The whole solids would be dissolved and reprecipitated within 1–4 years. The measured dissolution-precipitation rates of pure cement minerals give the maximum rate for ion substitution processes with contaminants and are distinguishable from faster processes such as surface complexation and ion exchange processes.


*Keywords:* Characterisation; Stability; Modelling; Waste management; Radiotracer

## 1. Introduction

The use of cement to stabilise waste and to immobilise contaminants is common practice for the disposal of many inorganic waste types. The chemical properties of cement systems, such as high pH, and gels and minerals with structures that may accommodate foreign ions are ideal for the immobilisation of many heavy metals and metalloid species. The major cement hydration products, calcium silicate hydrate (C-S-H) and calcium (sulfo)aluminate hydrates, are important for sorption and substitution [1,2]. Amorphous C-S-H may comprise >60% (w/w) of a cement [3] and has a high sorption potential because of its high specific surface area and variability in structure and composition [1]. Ion exchange reactions seem to be of little importance compared with the overall sorption on C-S-H phases [4].

The crystalline calcium sulfoaluminate hydrates, ettringite ($3CaO{\cdot}Al_2O_3{\cdot}3CaSO_4{\cdot}32H_2O$, an AFt phase), and monosulfate ($3CaO{\cdot}Al_2O_3{\cdot}CaSO_4{\cdot}12H_2O$, an AFm phase) favour crystallochemical substitution reactions [1]. Ettringite is formed as one of the first products during cement hydration [3]. Available solubility constants indicate that, in cement porewater, ettringite should be the more stable form of calcium sulfoaluminate hydrate. However, a mature cement paste may contain AFt or AFm or both phases. Both AFt and AFm phases have the ability to accept substitution of a number of anions and cations. The AFt phase is described by the general formula $C_6(A,F)X_3H_y$ ($C=CaO$, $A=Al_2O_3$, $F=Fe_2O_3$, $H=H_2O$), where $X$ represents one formula unit of a doubly charged anion or, with reservations, two formula units of a singly charged anion [3]. In addition to the $SO_4^{2-}$ end member ettringite, anionic substituted ettringites have been reported and synthesised for $AsO_4^{3-}$, $B(OH)_4^-$, $CO_3^{2-}$, $CrO_4^{2-}$, $NO^{3-}$, $OH^-$, $SeO_4^{2-}$, $SO_3^{2-}$, and $VO_4^{3-}$ [5–9]. Such extensive substitution and solid-solution formation is possible because of the column and channel-like structure of AFt [10] (Fig. 1). In contrast, AFm forms lamellar structured, hexagonal, or pseudohexagonal plates, with the general formula $C_4(A,F)X_2H_y$ (Fig. 1). Many different anions can serve as $X$, of which the most important for Portland cement hydration are $Cl^-$ (Friedel's salt), $OH^-$, $SO_4^{2-}$ (monosulfate), and $CO_3^{2-}$

* Corresponding author. Tel.: +41-1-823-5486; fax: +41-1-823-5210.
*E-mail address:* kellerbaur@freesurf.ch (I. Baur).
[1] Present address: Treetron GmbH, Umweltinformatik, Badenerstrasse 18, CH-8004 Zurich, Switzerland.

0008-8846/$ – see front matter © 2003 Elsevier Ltd. All rights reserved.
doi:10.1016/j.cemconres.2003.08.016

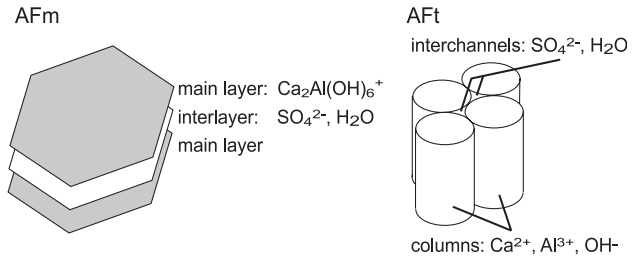


Fig. 1. Schematic representation of the lamellar AFm phase [3] and the column-like AFt phase [11].

[3]. In cementitious material, $B(OH)_4^-$, $CrO_4^{2-}$, $MoO_4^{2-}$, $SeO_4^{2-}$, and $SO_3^{2-}$ also have been shown to serve as interlayer anions [11–14]. Cation substitution for both AFt and AFm has been reported for $Al^{3+}$ with $Cr^{3+}$, $Mn^{3+}$, and $Ti^{3+}$ [15].

Although C-S-H, ettringite, and monosulfate have been shown to be important cement constituents for the immobilisation of hazardous components, their long-term leachability remains unclear. The binding of hazardous species can occur by ion exchange, by desorption, or, in the case of ion substitution, by dissolution-precipitation processes. The rates of these different processes vary. Ion exchange and sorption-desorption reactions usually occur within minutes to hours [16,17]. In contrast, dissolution-precipitation processes are much slower. They are likely to be particularly important for the soluble cement minerals according to the Ostwald Step Rule [18]. Dissolution rates reported in the literature for several minerals, including C-S-H, feldspars, and clays, are around $10^{-10}$ to $10^{-13}$ mol $m^{-2}$ $s^{-1}$ at pH 11–12 [19–21]. Under common experimental conditions and assuming that, at equilibrium, the dissolution rate equals the precipitation rate and the surface area remains unchanged, the time for a solid to be completely replaced (reconstruction time) will be weeks to years.

According to these considerations, knowledge of the dissolution-precipitation rates would be helpful for interpreting data obtained from sorption studies and, as a consequence, for predicting the long-term stability of ion-substituted cement minerals. However, such rates have not been determined for the above solids. In this paper, the dissolution-precipitation behaviour of pure ettringite, monosulfate, and C-S-H(I) phases at saturation was investigated by the use of radiotracers. Furthermore, a physical model was used to determine dissolution-precipitation rates.

## 2. Experiment

### 2.1. Materials

All chemicals were at least of p.a. grade. To prevent $CO_2$ contamination, all handling of material, the sampling, and the pH measurements were undertaken in a glovebox equipped with a $CO_2$ scrubber ($pCO_2 < 1$ ppm). Solutions were prepared using boiled ultrapure water (Millipore). Polyethylene (PE) bottles used for mineral synthesis were leached with acid (~ 0.1 M, diluted from concentrated $HNO_3$) for at least 24 h and rinsed with ultrapure water. The same procedure, but with a more diluted $HNO_3$ solution (pH ~ 4), was used to leach and rinse 0.45-μm nylon filters (Whatman).

### 2.2. Mineral synthesis

The C-S-H(I) phase (a structurally imperfect form of 1.4-nm tobermorite) was synthesised according to Atkins et al. [22] to achieve a Ca/Si ratio of 1. Ettringite was prepared by adding a solution of $Al_2(SO_4)_3 \cdot 18H_2O$ to a slurry of a stoichiometric amount of CaO in water at 4 °C in a 1-l PE bottle [23]. After a month of curing at room temperature, the solid phase was washed by centrifugation (10 min at 9000 rpm) and resuspension in water three times. The suspended solid was then subsequently filtered through 0.45-μm nylon filters and the filter cakes were dried in a $CaCl_2$-containing desiccator under continuous evacuation. For the synthesis of monosulfate, stoichiometric amounts of $(CaO)_3 \cdot Al_2O_3$ (prepared freshly according to Ref. [23]) and $CaSO_4 \cdot 2H_2O$ were mixed, cooled down to 4 °C, and suspended in cooled water (4 °C) at a water/solid ratio of 12 in a 1-l PE bottle. This slurry was shaken at 4 °C on a rotary shaker at 200 rpm for 48 h before curing for 5 months at room temperature. The washing procedure was the same as described for the ettringite, while the drying step of the monosulfate was gentler: the solid was filtered on a glass filter funnel. When the water suction was complete, acetone was filled into the funnel, mixed with the solid, and sucked off. This procedure was repeated three times. For the experiments only, the size fractions < 0.125 mm for AFt and AFm and < 63 μm for C-S-H(I) were used. The dried solids were stored in a desiccator over silica gel and soda lime.

### 2.3. Analytical methods

X-ray powder diffraction of the ground samples was performed with a Scintag XDS 2000 diffractometer (Cu*K*α radiation). The carbonate content of the solids was measured coulometrically [24]. Their stoichiometric composition was determined by X-ray fluorescence (Spectro X-lab 2000, S.D. < 0.5%). Aqueous Al and Ca concentrations were measured in acidified samples (1% [v/v] 65% $HNO_3$) by inductively coupled plasma-optical emission spectroscopy (ICP-OES; Spectroflame, Spectro Analytical Instruments, S.D. < 1%) and sulfate was measured using ion chromatography (Sykam) with a Sykam (AO4) column (S.D. < 2%). Scanning electron microscopy (SEM) investigations were performed with a Philips XL-30 (running at 25 kV, LaB6 filament). Before analysis, the specimens were coated with a platinum film. The specific surface area of the freshly prepared solids was determined by the BET method with a Carlo Erba Sorptomatic 1900 instrument [25]. Changes in

surface area of the hydrated phases under vacuum cannot be excluded.

### 2.4. Tracer experiments

The radiotracers $^{35}SO_4$ (as $Na_2SO_4$ in water) and $^{45}Ca$ (as $CaCl_2$ in water) were obtained from NEN Life Science and $^{32}Si$ (as $SiO_4^{4-}$ in 0.3-M NaOH) was from Los Alamos National Laboratory (USA). $^{35}S$, $^{45}Ca$, and $^{32}Si$ have half-lives of 87.5 days, 162.2 days, and ~100 years, respectively. The AFt and AFm suspensions were prepared at liquid/solid ratio (LS) of 500. Preliminary experiments have shown that equilibrium of AFt and AFm in water is reached after 7 days. To avoid major changes in the surface structure and the stoichiometry of the mineral phases during the equilibration process, the solids were suspended in 90% presaturated solutions with regard to AFt and AFm, respectively. The presaturated solutions were prepared by equilibrating suspensions (0.7 g $l^{-1}$ AFt and 1.1 g $l^{-1}$ AFm) for 7 days at room temperature on a rotary shaker (150 rpm), filtering through 0.45-μm nylon filters, and diluting to 90%. For the calcium sulfoaluminate hydrates, experiments with $^{35}SO_4$ and $^{45}Ca$ were performed in parallel. For C-S-H(I) experiments, presaturated solutions were prepared from $CaCl_2$, $SiCl_4$, and NaOH and the ionic strength was adjusted to 0.1 M using NaCl. The procedure is described in detail by Ref. [26]. To avoid unforeseen problems, the LS applied in this study (25,000) was the same as in the experiments of Ref. [26]. For C-S-H(I), the radiotracers $^{45}Ca$ and $^{32}Si$ were used. In a first series of experiments performed with the calcium sulfoaluminates only, radiotracers were added to presaturated solutions. To start the experiments at $t_0$, 25 ml of a tracer solution were added to 0.05 g of samples in 50-ml PE bottles. For blanks, no solid was added to labelled solutions. Both samples and blanks were performed in triplicate. In a second series of experiments, portions of solid (0.05 g) were suspended in 25-ml 90% presaturated solutions before the addition of the radiotracers and equilibrated at 22 ± 0.5 °C on a rotary shaker (150 rpm) for 7 days. To start the experiments at $t_0$, 1 ml of a tracer solution was added to samples (equilibrated suspensions) and blanks (only presaturated solutions), each in triplicate. Tracer solutions were diluted before the experiments to keep the addition of $SO_4$, Ca, and Si as small as possible (< 0.005% of the total amount in solution for $SO_4$ and Ca and < 1% for Si) but still sufficient to detect the tracer. After between 1 and 70 days (first series) and 1 and 44 days (second series) at 22 ± 0.5 °C on a rotary shaker (150 rpm), 20 ml of sample were removed by a syringe and filtered through a 0.45-μm nylon syringe filter (25 mm, TITAN). A portion of the filtrate (5 ml) was then mixed with 10-ml scintillation cocktail (Insta-Gel Plus, Packard) in 20-ml HDPE scintillation vials (986710, Wheaton) and counted in a liquid scintillation analyser (Tri-Carb 2200CA, Packard). The measured activity corresponded to the total amount of tracer added, so sorption to reaction vessels was not significant. The percentage uptake ($U_i$) of a radiotracer of the component $i$ by the solid was calculated as follows:

$$U_i = 1 - \left(\frac{n_{i(\mathrm{aq})}(S)}{n_{i(\mathrm{aq})}(B)}\right) \times 100 \quad [\%] \tag{1}$$

where $n_{i(\mathrm{aq})}(S)$ and $n_{i(\mathrm{aq})}(B)$ are the counts (in cpm) of the component $i$ in the samples and the corresponding blanks, respectively. In the second series, two extra samples were performed for each suspension without tracer addition. They were filtered at $t_0$ and after 44 days, respectively. The filter cakes were air-dried and stored in a desiccator before analysis by SEM and XRD.

### 2.5. Determination of dissolution-precipitation rates

In the case of a congruently dissolving solid in equilibrium with a solution, the ratio $r$ of each of its components $i$ in the solid, $c_{i(\mathrm{s})}$, to the total amount in the batch, $c_{i(\mathrm{tot})}$, is constant for all components:

$$r_i = \frac{c_{i(\mathrm{s})}}{c_{i(\mathrm{tot})}} \quad [-] \tag{2}$$

When an amount of radiotracer of a component, $n_i$, is added to this system, its distribution in the solid and solution will, after infinite time, equal $r_i$ at equilibrium. To describe the processes when a radiotracer is added to a batch, we used the following physical model:

$$n_{i(\mathrm{aq})} \underset{k1}{\overset{k2}{\rightleftarrows}} n_{i(\mathrm{s})} \quad [\mathrm{cpm}] \tag{3}$$

where $n_{i(\mathrm{aq})}$ and $n_{i(\mathrm{s})}$ are the amounts of tracer in solution and in the solid, respectively (in cpm), $k_1$ is the dissolution coefficient (cpm days $^{-1}$), and $k_2$ the tracer uptake rate (days $^{-1}$). The change of $n_{i(\mathrm{aq})}$ with time depends on $k_{i,1}$ and $k_{i,2}$:

$$\frac{\partial n_{i(\mathrm{aq})}}{\partial t} = k_{i,1} - k_{i,2} \cdot n_{i(\mathrm{aq})}(t) \quad [\mathrm{cpm\ days}^{-1}] \tag{4}$$

For $((\partial n_{i(\mathrm{aq})})/(\partial t)) = 0$ follows:

$$n_{i(\mathrm{aq}),\mathrm{eq}} = \frac{k_{i,1}}{k_{i,2}} \quad [\mathrm{cpm}] \tag{5}$$

where $n_{i(\mathrm{aq}),\mathrm{eq}}$ is equal to the amount of tracer in solution, when equilibrium is reached. $n_{i(\mathrm{aq}),\mathrm{eq}}$ is related to $r_i$ by:

$$r_i = 1 - \frac{n_{i(\mathrm{aq}),\mathrm{eq}}}{n_{i(\mathrm{aq}),0}} \quad [-] \tag{6}$$

where $n_{i(\mathrm{aq}),0}$ is the amount of tracer in solution in cpm at the beginning ($t_0$).

Integrating and solving Eq. (4) for $n_i(t)$ gives:

$$n_{i(\mathrm{aq})}(t) = \frac{k_{i,1}}{k_{i,2}} + \left(n_{i(\mathrm{aq}),0} - \frac{k_{i,1}}{k_{i,2}}\right) e^{-k_{i,2}t} \quad \text{or, using Eq. (5),}$$

$$n_{i(\mathrm{aq})}(t) = n_{i(\mathrm{aq}),\mathrm{eq}} + (n_{i(\mathrm{aq}),0} - n_{i(\mathrm{aq}),\mathrm{eq}}) e^{-k_{i,2}t} \quad [\mathrm{cpm}] \tag{7}$$

Taking the natural logarithm of Eq. (7) results in a linear relation:

$$\ln(n_{i(\mathrm{aq})}(t) - n_{i(\mathrm{aq}),\mathrm{eq}}) = \ln(n_{i(\mathrm{aq}),0} - n_{i(\mathrm{aq}),\mathrm{eq}}) - k_{i,2}t \qquad (8)$$

The decrease in tracer counts of the measured values $n_{i(\mathrm{aq})}(S_t)$ was corrected with the ratio of the counts in the blank at $t_0$ to the counts at the time of sampling:

$$n_{i(\mathrm{aq})}(t) = n_{i(\mathrm{aq})}(S_t)\frac{n_{i(\mathrm{aq})}(B_0)}{n_{i(\mathrm{aq})}(B_t)} \quad [\mathrm{cpm}] \qquad (9)$$

Plotting the left term of Eq. (8) against time results in a linear relation with the slope $-k_{i,2}$, the tracer uptake rate. $k_{i,2}$ was determined from the linear regression of the data set. The dissolution rate at saturation, $k_{i,1}$, was calculated based on Eq. (5) and converted to mol $m^{-2}$ $s^{-1}$ by use of the specific activity (cpm $mol^{-1}$) and the specific surface area ($m^2$).

## 3. Results and discussion

### 3.1. Phase characterisations

The XRD spectra of the synthetic phases indicated that a pure ettringite had been obtained, while the synthetic monosulfate contained some ettringite impurity (Fig. 2). The data of the synthetic C-S-H(I) phase were in good agreement with those published in Ref. [3]. In all three solids, a small carbonate contamination on the order of $<0.05\%$ C (w/w) was measured. Specific surface areas for ettringite, monosulfate, and C-S-H(I) were 9.8, 5.7, and 41.0 $m^2$ $g^{-1}$, respectively (S.D. $<3\%$). The elemental composition of the solids is stoichiometric (Table 1). Table 1 also gives the solubility data for the solids. The determined ratios $r_i$ for the given experimental conditions (Eq. (2)), are presented in Table 2. In ettringite, $r_{\mathrm{Ca}}$ and $r_{\mathrm{SO4}}$ agree, as it was assumed for a congruently dissolving solid (Eq. (2)), whereas the ratios $r_i$ for the components of the noncongruently dissolving solids, monosulfate and C-S-H(I), differed significantly. The dissolution of the thermodynamically unstable monosulfate led to the precipitation of ettringite as described by Atkins et al. [23], clearly illustrated in the SEM micrograph of equilibrated monosulfate as needles among monosulfate platelets (Fig. 3B). These ettringite precipitates were also observed in XRD spectra taken of the equilibrated samples by the intensified peaks at 9° and 15.8° 2$\theta$ ($d$-spacings 9.7 and 5.6 Å; data not shown) compared with the nonequilibrated monosulfate spectrum (Fig. 2).

Table 1
Elemental composition of the synthetic ettringite, monosulfate, and C-S-H(I) and their concentrations (mmol $l^{-1}$) in solution at equilibrium ($T=25$ °C)

| | Ca | Al | $SO_4$ | pH at equilibrium |
|---|---|---|---|---|
| Ettringite | | | | |
| Theoretical | 6 | 2 | 3 | |
| In solid | 6 | $1.94 \pm 0.01$ | $3.11 \pm 0.19$ | |
| In solution | 6 | $2.14 \pm 0.13$ | $3.19 \pm 0.17$ | $11.02 \pm 0.02$ |
| | $2.06 \pm 0.13$ | $0.735 \pm 0.045$ | $1.14 \pm 0.13$ | |
| Monosulfate | | | | |
| Theoretical | 4 | 2 | 1 | |
| In solid | 4 | $1.93 \pm 0.03$ | $1.16 \pm 0.16$ | |
| In solution | 4 | $2.69 \pm 0.37$ | $0.02 \pm 0.002$ | $11.69 \pm 0.04$ |
| Concentration | $4.75 \pm 0.49$ | $3.20 \pm 0.28$ | $0.024 \pm 0.002$ | |
| | Ca | Si | | pH at equilibrium |
| C-S-H(I) | | | | |
| Theoretical | 1 | 1 | | |
| In solid | 1 | $0.98 \pm 0.003$ | | |
| In solution | 1 | $0.04 \pm 0.02$ | | $11.76 \pm 0.05$ |
| | $2.75 \pm 0.12$ | $0.12 \pm 0.006$ | | |

The data are normalised to 6 moles of Ca for ettringite, 4 moles of Ca for monosulfate, and 1 mole of Ca for C-S-H(I). The uncertainty indicates the $2\sigma$ error of the measurements.

### 3.2. Tracer uptake behaviour and dissolution-precipitation rates

Because of their larger specific surface area, finely divided solids have a greater solubility than large crystals

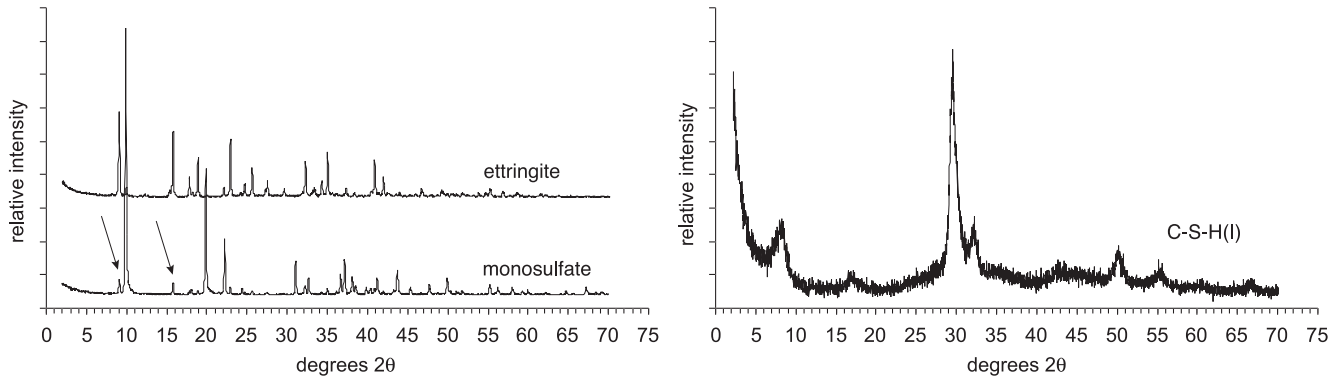


Fig. 2. XRD pattern of the synthetic ettringite, monosulfate, and C-S-H(I). The arrows mark the ettringite peaks at 9° and 15.8° (2$\theta$ $d$-spacings 9.7 and 5.6 Å) found in the monosulfate pattern (Cu$K\alpha$ radiation).

Table 2
Determined ratios $r_i$ for the amount of component $i$ in the solid, $c_{i(s)}$, to the total amount of $i$ in the batch, $c_{i(tot)}$, in ettringite, monosulfate, and C-S-H(I)

| $i=$ | $r_i = c_{i(s)}/c_{i(tot)}$ | | |
|---|---|---|---|
| | Ca | $SO_4$ | Si |
| Ettringite | $0.83 \pm 0.01$ | $0.81 \pm 0.02$ | |
| Monosulfate | $0.72 \pm 0.02$ | $0.99 \pm 0.004$ | |
| C-S-H(I) | $0.10 \pm 0.004$ | | $0.72 \pm 0.01$ |

The uncertainty indicates the $2\sigma$ error of the measurements.

[27]. As a consequence, small crystals are thermodynamically less stable and should recrystallise into large ones. However, the crystal size and surface structure at $t_0$ and $t_{44}$ appear to be very similar in the SEM micrographs taken of the second series of samples (Fig. 3). It is possible that the shaking of the samples inhibited the growth of larger crystals. In consequence, it was assumed that the overall surface area stayed constant during the second series of experiments. In the first series of experiments, constant surface area can be assumed similarly for the time from 7 days after suspending the solid in the labelled solution ($t_7$), when equilibration was reached. However, the specific surface areas of the freshly synthesised solids were used as conversion factors for $k_1$ (see Section 2.4) and possible methodological errors in determining these values or changes with time cannot be accounted for.

During the first days of equilibration, tracer uptake was much higher than afterwards (Fig. 4). This indicates fast processes at the beginning, such as rapid dissolution-precipitation rates due to the dissolution of fine particles or adsorption-desorption. In the second series of experiments, started with already equilibrated suspensions, the initial fast uptake was much lower but still evident. It seems that the

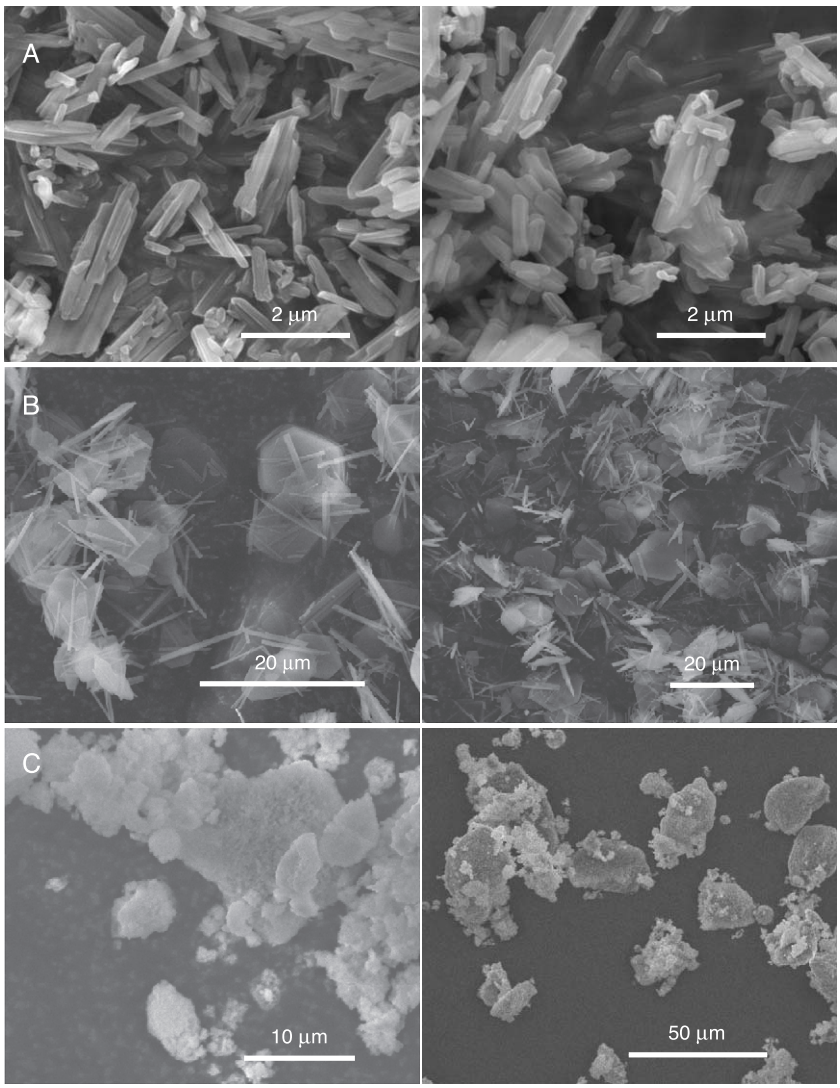


Fig. 3. SEM micrographs of the dried solids taken at the beginning ($t_0$, left) and the end ($t_{44}$, right) of the sampling period of the second series of experiments. There appears to be no change in crystal size and surface structure. A, ettringite; B, monosulfate; C, C-S-H(I).

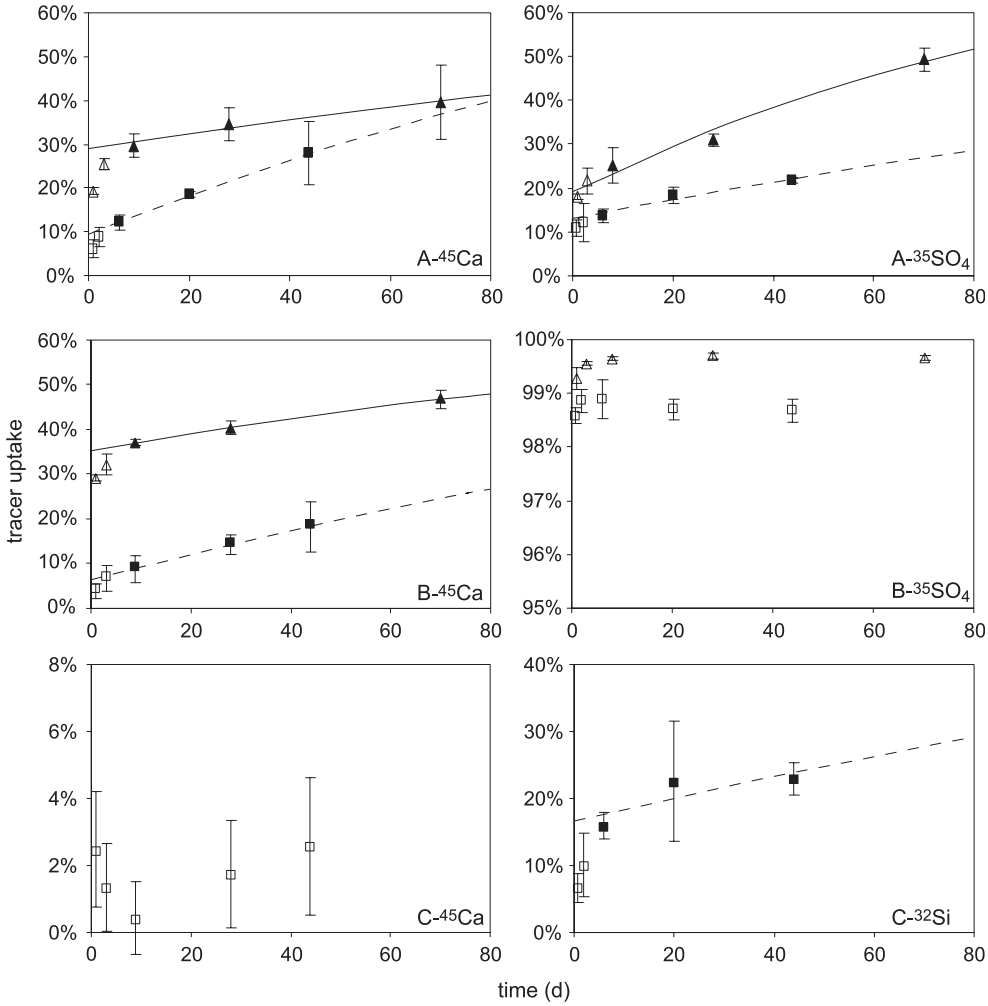


Fig. 4. Percentage radiotracer uptake from solution, $U_i = \left(1 - \left((n_{i(\mathrm{aq})}(S))/(n_{i(\mathrm{aq})}(B)\right)\right) \times 100$, against time into solid in equilibrated ettringite (A), monosulfate (B), and C-S-H(I) (C) suspensions (pH 11.02, 11.69, and 11.76, respectively), showing the measured values in the first series of experiments (▲), the measured values in the second series of experiments (■), and the data points not included in the fitting (△, □). The solid line represents the fitted model to first series of data points and the dashed line represents the fitted model to second series of data points. The errors ($2\sigma$) are shown.

added amount of tracer, although small, disturbed the equilibrium and caused a precipitation. As a consequence, only the data points after $t_7$ were used in both experimental series to model the tracer uptake rates, $k_2$, and the dissolution coefficients, $k_1$. The modelled curves are presented in Fig. 4. The calculated values $k_2$ and $k_1$, as well as the predicted reconstruction time of the solids, the time when the whole solid will have undergone dissolution and reprecipitation, are presented in Table 3. The model fits the data points well in the case of the calcium sulfoaluminates. The determined rates for the first and second series of experiments seem different for Ca and $SO_4$ in ettringite. Different components in the same solid should behave identically in a congruent dissolution-precipitation process. However, the values are in the same order of magnitude, and taking into account the error bars of the data points in Fig. 4, the differences seem to be a result of the uncertainty of the measurements. The determined reconstruction time for ettringite lay within 1.2–4 years, which resulted in a dissolution-precipitation rate of $10^{-12.2}$ to $10^{-11.5}$ mol $m^{-2}$ $days^{-1}$. For monosulfate, the data for the two series for $^{45}Ca$ agreed well, both resulting in a reconstruction time around 500 days. The dissolution-pre-

Table 3
Determined tracer uptake rates, $k_{i,2}$, and dissolution-precipitation rates, $k_{i,1}$

| | $i$ | $k_{i,2}$ ($10^{-3}$ $days^{-1}$) | log $k_{i,1}$ (mol $m^{-2}$ $s^{-1}$) | Reconstruction time (days) |
|---|---|---|---|---|
| Ettringite | Ca (1) | 3.26 ± 1.15 | − 12.15 ± 0.15 | 1445 ± 552 |
| | Ca (2) | 6.60 ± 0.03 | − 11.86 ± 0.02 | 736 ± 108 |
| | $SO_4$ (1) | 9.38 ± 2.56 | − 11.65 ± 0.12 | 459 ± 142 |
| | $SO_4$ (2) | 3.25 ± 1.51 | − 12.12 ± 0.20 | 1348 ± 656 |
| Monosulfate | Ca (1) | 5.31 ± 0.10 | − 11.17 ± 0.03 | 501 ± 69 |
| | Ca (2) | 4.65 ± 0.17 | − 11.23 ± 0.03 | 575 ± 81 |
| C-S-H(I) | Si (2) | 3.23 ± 4.67 | − 11.56 ± 0.63 | 789 ± 1139 |

The reconstruction time represents the predicted time when 100% of the solid has undergone dissolution and reprecipitation for the components of ettringite, monosulfate, and C-S-H(I). (1) First series of experiments. (2) Second series of experiments. The uncertainty indicates the $2\sigma$ error of the measurements.

cipitation rate presented in Table 3 for monosulfate must, however, be considered with care because ettringite forms during suspension with an accompanying change in specific surface area. The $^{35}SO_4$ uptake in monosulfate was very fast and reached $r_{SO4}$ ( ~ 99%) in both series within 1 day. Thus, the $^{35}SO_4$ dissolution-precipitation rate could not be modelled. This immediate uptake of $^{35}SO_4$ was most probably caused by ion exchange with the weakly bound interlayer sulfate.

The $^{45}Ca$ uptake for C-S-H(I) was not modelled, because it was so low relative to the uncertainty of the data points. In addition, for $^{32}Si$, the uncertainty of the measurements was high, resulting in a dissolution-precipitation rate with a considerable error. Schweizer [21] determined a C-S-H(I) dissolution rate of $10^{-10.5}$ mol $m^{-2}$ $days^{-1}$ using a flow-through experiment far from equilibrium at pH 12 and congruent dissolution. The dissolution-precipitation rate modelled in this study is one order of magnitude lower. However, this value is determined at saturation, where rates are expected to be lower [27].

The results presented give a good overview over the stability of the solids and the dissolution-precipitation processes occurring in suspension. The dissolution-precipitation rates obtained for ettringite and monosulfate, which represent a maximum rate for ion substitution processes with contaminants, can be used to distinguish this processes from comparably fast reactions, such as surface complexation and ion exchange, from ion substitution in sorption studies. It should be noted, however, that only C-S-H with a Ca/Si ratio of 1 was investigated. Because C-S-H has such a large structural flexibility, it is possible that dissolution-precipitation rates vary quite strongly with Ca/Si ratio. In addition, as has been shown for $Zn^{2+}$ [26], ions may slowly diffuse into interlayers or internal surfaces without $Ca^{2+}$ release. Such a diffusion process would be difficult to discern from the dissolution-precipitation reaction rate for C-S-H(I).

In summary, the dissolution-precipitation rates can be distinguished from ion exchange and adsorption, but not necessarily from rates, where a contaminant diffuses into a solid phase, where it may undergo incorporation into a crystal structure. However, for a contaminant to be built into a crystal structure as a consequence of dissolution-precipitation processes, the resulting mineral must be thermodynamically more stable than the original cement mineral. Both kinetic and thermodynamic approaches must be considered for each contaminant species to understand its binding mechanism.

## Acknowledgements

The authors gratefully acknowledge the funding of the Swiss Federal Institute of Environmental Science and Technology (EAWAG) and the assistance of Laura Canonica and Hermann Moench.

## References

[1] F.P. Glasser, in: R.D. Spence (Ed.), Chemistry and Microstructure of Solidified Waste Forms, Lewis Publishers, Boca Raton, FL, 1993, pp. 1–40.
[2] M.L.D. Gougar, B.E. Scheetz, D.M. Roy, Ettringite and C-S-H Portland cement phases for waste ion immobilization: a review, Waste Manage. 16 (1996) 295–303.
[3] H.F.W. Taylor, Cement Chemistry, Thomas Telford, London, 1997.
[4] S. Komarneni, E. Breval, D.M. Roy, R. Roy, Reactions of some calcium silicates with metal cations, Cem. Concr. Res. 18 (1988) 204–220.
[5] P. Kumarathasan, G.J. McCarthy, D.J. Hassett, D.F. Pflughoeft-Hasset, Oxyanion substituted ettringites: Synthesis and characterization; and their potential role in immobilization of As, B, Cr, Se and V, Mater. Res. Soc. Symp. Proc. 178 (1990) 83–104.
[6] G.J. McCarthy, D.J. Hassett, J.A. Bender, Synthesis, crystal chemistry and stability of ettringite, a material with potential applications in hazardous waste immobilization, Mater. Res. Soc. Symp. Proc. 245 (1992) 129–140.
[7] H. Pöllmann, S. Auer, H.-J. Kuzel, Solid solution of ettringites: part II. Incorporation of $B(OH)_4^-$ and $CrO_4^{2-}$ in $3CaO{\cdot}Al_2O_3{\cdot}3CaSO_4{\cdot}32H_2O$, Cem. Concr. Res. 23 (1993) 422–430.
[8] S.C.B. Myneni, S.J. Traina, T.J. Logan, G.A. Waychunas, Oxyanion behavior in alkaline environments: sorption and desorption of arsenate in ettringite, Environ. Sci. Technol. 31 (1997) 1761–1768.
[9] R.B. Perkins, C.D. Palmer, Solubility of $Ca_6[Al(OH)_6]2(CrO_4)_3{\cdot}26H_2O$, the chromate analog of ettringite; 5–75 °C, Appl. Geochem. 15 (2000) 1203–1218.
[10] A.W. Moore, H.F.W. Taylor, Crystal structure of ettringite, Acta Crystallogr. B Struct. Sci. 26 (1970) 386–393.
[11] A. Kindness, E.E. Lachowski, A.K. Minocha, F.P. Glasser, Immobilisation and fixation of molybdenum (VI) by Portland cement, Waste Manage. 14 (1994) 97–102.
[12] M. Zhang, Incorporation of oxyanionic B, Cr, Mo, and Se into hydrocalumite and ettringite: Application to cementitious systems, PhD thesis, University of Waterloo, Canada, 1995.
[13] H. Motzet, H. Pöllmann, Synthesis and characterisation of sulfite-containing AFm phases in the system $CaO\text{-}Al_2O_3\text{-}SO_2\text{-}H_2O$, Cem. Concr. Res. 29 (1999) 1005–1011.
[14] R.B. Perkins, C.D. Palmer, Solubility of chromate hydrocalumite $(3CaO{\cdot}Al_2O_3{\cdot}CaCrO_4{\cdot}nH_2O)$ 5–75 °C, Cem. Concr. Res. 31 (2001) 983–992.
[15] J. Bensted, S. Prakash Varma, Studies of ettringite and its derivatives: part 4. The low sulphate form of calcium sulphoaluminate (monosulphate), Cem. Technol. 4 (1973) 112–116.
[16] G. Sposito, in: J.A. Davis, K.F. Hayes (Eds.), Geochemical Processes at Mineral Surfaces, American Chemical Society, Washington, 1986, pp. 217–228.
[17] G. Sposito, Chemical Equilibria and Kinetics in Soils, Oxford Univ. Press, New York, 1994.
[18] R.A. van Santen, The Ostwald Step Rule, J. Phys. Chem. 88 (1984) 5768–5769.
[19] A.F. White, S.L. Brantley (Eds.), Chemical Weathering Rates of Silicate Minerals, vol. 31, Mineralogical Society of America, Chelsea, MI, 1995, pp. 407–461.
[20] F.J. Huertas, L. Chou, R. Wollast, Mechanism of kaolinite dissolution at room temperature and pressure: part II. Kinetic study, Geochim. Cosmochim. Acta 63 (1999) 3261–3275.
[21] C. Schweizer, Calciumsilikathydrat-Mineralien. Lösungskinetik und ihr Einfluss auf das Auswaschverhalten von Substanzen aus einer Ablagerung mit Rückständen aus Müllverbrennungsanlagen, PhD thesis, Swiss Federal Institute of Technology (ETH), Zürich, 1999.
[22] M. Atkins, F.P. Glasser, A. Kindness, Cement hydrate phases: Solubility at 25 °C, Cem. Concr. Res. 22 (1992) 241–246.
[23] M. Atkins, D. Macphee, A. Kindness, F.P. Glasser, Solubility proper-

ties of ternary and quaternary compounds in the $CaO-Al_2O_3-SO_3-H_2O$ system, Cem. Concr. Res. 21 (1991) 991–998.
[24] E.W.D. Huffman, Performance of a new automatic carbon dioxide coulometer, Microchem. J. 22 (1977) 567–573.
[25] S. Brunnauer, P.H. Emmet, E. Teller, Adsorption of gases in multimolecular layers, J. Am. Chem. Soc. 60 (1938) 309–319.
[26] F. Ziegler, R. Gieré, C.A. Johnson, Sorption mechanisms of zinc to calcium silicate hydrate: sorption and microscopic investigations, Environ. Sci. Technol. 35 (2001) 4556–4561.
[27] W. Stumm, Chemistry of the Solid–Water Interface, Wiley, New York, 1992.